

# Modular Response in Free Quantum Fields: A KMS/FDT Theorem and Conditional Extensions

[c]g<sup>1</sup>  
<sup>1</sup>[Institutions]  
 (Dated:)

**Part I (Theoremic core, free/Gaussian Hadamard QFT).** We prove that, for small causal diamonds (CHM) in locally Hadamard states and within a safe window  $\epsilon_{UV} \ll \ell \ll \min\{L_{\text{curv}}, \lambda_{\text{mfp}}, m_i^{-1}\}$ , the MI/moment-kill projector isolates a finite  $\ell^4$  modular response with coefficient equal to its flat-space value; the projected KMS/FDT susceptibility is positive; and coarse-graining over the wedge family produces the universal weak-field prefactor  $5/12 = (4/3) \times (5/16)$ . The fractional KMS defect between CHM diamonds and half-spaces scales as  $\mathcal{O}((\ell/L_{\text{curv}})^2) + \mathcal{O}((\ell H)^2)$ . The QFT sensitivity is  $\beta = 2\pi C_T I_{00} = 0.02086 \pm 0.00105$  (conservative 5% shared systematics from four independent routes). A scheme-invariant background relation *suggests*  $\Omega_\Lambda = \beta f c_{\text{geo}}$  *conditional* on our coarse-graining and analyticity assumptions.

**Part II (Conditional extensions).** We separate *definition* (flat-space  $\epsilon$  from modular response) from *mapping*. Rather than impose the standard EFT-of-DE  $\alpha$ -basis, we adopt a quasi-static closure that keeps operational distances GR-like (no additional lensing coupling  $\Sigma \simeq 1$ ) while modifying growth via  $\mu(\epsilon, s) = 1/(1 + \frac{5}{12}\epsilon s(x))$  with  $s(x)$  a local, covariant environment modulation derived from the action. We supply a frame-independence remark and an action-level realization of  $s(x)$ . KMS/FDT positivity motivates an entropy-driven law  $d\epsilon/d \ln a \geq 0$  with a *conditional* background budget  $\int \epsilon d \ln a = \Omega_\Lambda$ . Cosmological illustrations ( $S_8$  band and  $H_0$  bounds) are **toy/illustrative** and propagate the  $\pm 5\%$   $\beta$  uncertainty; *observed lensing amplitudes still reflect the altered growth*.

**Part III (Exploratory).** (i) An *optional*, shock-selective *optical* channel (Assumption D') reduces  $\Sigma$  only in high-shear shocked gas to address Bullet-type lensing offsets while preserving FRW distances. We retain a simple local saturating law in the text, and now provide a *principled derivation path* from Schwinger–Keldysh (SK) hydrodynamics that makes  $\alpha_{\text{opt}}$  a calculable function of ICM transport coefficients (App. XXIII). (ii) A compact thermodynamic interpretation of the projected modular response: a Clausius-like identity holds at working order in the MI/moment-kill channel, and the FRW budget may be viewed as a *coarse-grained* Clausius normalization *conditional* on our KMS→FRW hypotheses. We clarify the relation to the Casini–Galante–Myers critique of Jacobson.

## READER’S MAP: PART I (THEOREM) VS. PART II (CONDITIONAL) VS. PART III (EXPLORATORY)

**Part I (Secs. I–IV, Apps. XV–XVIII):** proven results for free/Gaussian Hadamard fields at working order.

**Part II (Secs. V–XXIV, Apps. XIX–XX, XXI):** conditional extensions, Assumptions C & D (stated), safe-window fraction, KMS→FRW link, *action-derived* environment modulation, entropic sketch, and toy/illustrative numerics with propagated uncertainties.

**Part III (Secs. VII C, XIII, App. XXIII):** exploratory shock-selective optical response (Assumption D') with an SK/BRSSS derivation path and a thermodynamic interpretation (Clausius form in the projected channel; conditional FRW budget) and relation to CGM’s critique of Jacobson.

## I. SCOPE, WORKING ORDER, AND SAFE-WINDOW QUANTIFICATION (PART I)

*a. Working order and state class.* We work to  $\mathcal{O}(\ell^4)$  in the MI/moment-kill projector channel, treating curvature/contact terms as  $\mathcal{O}(\ell^6)$ . States are locally Hadamard.

*b. KMS applicability (CHM diamonds).* Exact BW KMS holds for half-spaces; CHM diamonds inherit it with fractional defect  $\mathcal{O}((\ell/L_{\text{curv}})^2) + \mathcal{O}((\ell H)^2)$  (App. XVIII).

*c. Safe-window volume fraction.* Define a conservative admissible scale

$$\ell_{\text{max}}(x) \equiv \zeta \min \left\{ L_{\text{curv}}(x), \lambda_{\text{mfp}}(x), m_i^{-1}(x) \right\}, \quad \zeta = 0.1. \quad (1)$$

Using Press–Schechter/Sheth–Tormen mass functions and NFW curvature proxies  $L_{\text{curv}}^{-2} \sim (R_{abcd} R^{abcd})^{1/2}$  with substructure excision parameter  $\xi$ , we estimate the comoving volume fraction  $f_V(\ell_{\text{min}}) = \text{Vol}\{x : \ell_{\text{max}}(x) > \ell_{\text{min}}\} / \text{Vol}_{\text{tot}}$ . A semi-analytic survey (App. XIX) shows voids dominate  $f_V$ , while dense cores lack a window; representative values at  $z \sim 0$  for  $\ell_{\text{min}} \in [1, 100]$  pc are  $f_V \sim 0.6\text{--}0.95$  for  $\xi \in [0.2, 0.5]$ . This enters only as a domain-of-validity indicator.

*d. Spectrum caveat.* The admissible window  $\epsilon_{UV} \ll \ell \ll \min\{L_{\text{curv}}, \lambda_{\text{mfp}}, m_i^{-1}\}$  is understood to apply to sectors that contribute at working order. Massive sectors with  $\ell \gg m_i^{-1}$  are exponentially suppressed and, after MI/moment-kill subtraction, do not re-introduce lower moments or  $\ell^4 \log \ell$  terms. Thus the  $\ell^4$  coefficient is dominated by massless/light fields while heavy fields decouple in this channel.

*e. Angle invariance as a null test.* The continuous-angle product  $\mathcal{C}_\Omega = f(\theta) c_{\text{geo}}(\theta)$  is analytic and  $\theta$ -independent; residuals are shown as a null check, not a precision claim.

## II. A2-KMS THEOREM (GAUSSIAN/HADAMARD SECTOR)

**Theorem 1** (Projected modular response and positivity). *Let  $\mathcal{Q}$  be a free (Gaussian) QFT on a globally hyperbolic spacetime and  $\rho$  a locally Hadamard state. For a causal diamond of radius  $\ell$  with  $\ell \ll L_{\text{curv}}$  and the MI/moment-kill projector that cancels  $r^0$  and  $r^2$  moments, the MI-subtracted modular response obeys*

$$\delta\langle K_{\text{sub}} \rangle = (2\pi C_T I_{00}) \ell^4 \delta\epsilon + \mathcal{O}(\ell^6), \quad (2)$$

*with coefficient equal to the flat-space value. The retarded susceptibility  $\chi_{QK}$  in the projected channel is positive (FDT), and wedge averaging yields the universal weak-field prefactor  $5/12$ . The fractional deviation from BW KMS is  $\mathcal{O}((\ell/L_{\text{curv}})^2) + \mathcal{O}((\ell H)^2)$ .*

**Corollary 1** (Conditional background statement). *Under the coarse-graining and analyticity assumptions of Sec. VI, the FRW zero mode suggests the scheme-invariant relation  $\Omega_\Lambda = \beta f c_{\text{geo}}$  with  $\beta = 2\pi C_T I_{00}$ . We treat this as a conditional statement rather than a theorem.*

## III. QFT INPUT: $\beta = 2\pi C_T I_{00}$ AND ERROR BUDGET

We evaluate  $\beta$  via four independent routes: (a) real-space CHM; (b) spectral/Bessel; (c) Euclidean time-slicing; (d) replica finite-difference. The spread is  $\lesssim 1\%$ . We adopt a conservative

$$\beta = 0.02086 \pm 0.00105 \quad (5\% \text{ shared systematics}). \quad (3)$$

Angle invariance is used as a null residual test.

Here  $C_T$  denotes the flat-space stress-tensor two-point normalization, e.g.  $\langle T_{ab}(x) T_{cd}(0) \rangle = C_T \mathcal{I}_{abcd}(x)/|x|^{2d}$  in  $d$  dimensions (see Osborn–Petkou).

*Benchmark (convention).* For a free, massless real scalar in  $d = 4$  and our normalization,  $C_T = 1/(120\pi^2)$ , which yields  $\beta \simeq 0.02086$  via Eq. (4).

**Implementation consistency (note).** The normative constants used for the numerical reproductions are

$$C_T = \frac{1}{120\pi^2}, \quad (\sigma_1, \sigma_2) = \left(\frac{1}{2}, 2\right), \quad (a, b) = \left(\frac{4}{5}, \frac{1}{5}\right),$$

with the moment-kill identities enforced exactly (App. XV). Helper scripts (`beta_methods_v2.py`, `referee_pipeline.py`) print these values alongside the computed  $I_{00}$  to prevent normalization drift.<sup>1</sup>

**Reproducibility (non-circular).** We use a two-scale MI/moment-kill subtraction with a top-hat window on 3-balls

$$W_\ell(r) = \frac{3}{4\pi\ell^3} \Theta(\ell - r), \quad \mathcal{W}_\ell := \int_{B_\ell} W_\ell - a \int_{B_{\sigma_1\ell}} W_{\sigma_1\ell} - b \int_{B_{\sigma_2\ell}} W_{\sigma_2\ell}.$$

The two moment-kill conditions (cancelling  $r^0$  and  $r^2$  for any smooth radial  $F$ ) fix

$$a + b = 1, \quad a\sigma_1^2 + b\sigma_2^2 = 1 \implies a = \frac{\sigma_2^2 - 1}{\sigma_2^2 - \sigma_1^2}, \quad b = \frac{1 - \sigma_1^2}{\sigma_2^2 - \sigma_1^2}.$$

In our runs we take

$$(\sigma_1, \sigma_2) = \left(\frac{1}{2}, 2\right), \quad (a, b) = \left(\frac{4}{5}, \frac{1}{5}\right) = (0.8, 0.2).$$

<sup>1</sup> In earlier development branches some convenience flags defaulted to alternate normalizations (e.g.  $C_T = 3/\pi^4$ ) and near-unity MI scales. These have been disabled in the archival runners; the paper's conventions are authoritative.

With these weights the projected  $\ell^4$  coefficient evaluates to

$$I_{00} = 3.932017 \text{ (dimensionless),}$$

so with  $C_T = 1/(120\pi^2)$  one obtains  $\beta = 2\pi C_T I_{00} = 0.02086$  as quoted. The helper script `beta_methods_v2.py` echoes both  $(a, b; \sigma_1, \sigma_2)$  and the numeric  $I_{00}$ .

#### IV. WEAK-FIELD PREFACTOR 5/12

The isotropic BW channel gives  $\langle T_{kk} \rangle = (1 + w)\rho$  with UV  $w = 1/3 \Rightarrow 4/3$ . Averaging over CHM segments yields  $5/16$ , so  $5/12 = (4/3) \times (5/16)$ . Details in App. XVII.

#### V. DEFINITION VS. MAPPING (PART II; CONDITIONAL)

*a. Definition (flat-space QFT).*

$$\delta\langle K_{\text{sub}}(\ell) \rangle = \underbrace{(2\pi C_T I_{00})}_{\beta} \ell^4 \delta\varepsilon(x) + \mathcal{O}(\ell^6). \quad (4)$$

*b. Mapping (constitutive; beyond the  $\alpha$ -basis).* We *do not* impose the linear EFT-of-DE  $\alpha$ -parameter mapping at working order. Instead, we adopt a quasi-static closure that keeps operational distances GR-like while modifying growth:

$$\nabla^2 \Phi = 4\pi G a^2 \rho_m \mu(\varepsilon, s), \quad \mu(\varepsilon, s) = \frac{1}{1 + \frac{5}{12}\varepsilon s(x)}, \quad (5a)$$

$$\nabla^2 \frac{\Phi + \Psi}{2} = 4\pi G a^2 \rho_m, \quad (\Sigma \simeq 1 \text{ on FRW and in laminar flows}). \quad (5b)$$

Here  $s(x)$  is a local scalar built from curvature (Sec. IX); in FRW,  $\text{Weyl} = 0 \Rightarrow \chi_g = 0 \Rightarrow s = 1$ . *Beyond working order we make no stability claims absent an action;  $\mu(\varepsilon, s)$  serves as a falsifiable diagnostic with  $\Sigma \simeq 1$ .* Matter obeys the standard continuity and Euler equations. This closure preserves the Bianchi identity at working order because  $s(x)$  is a scalar; an action-level realization and frame-independence are given below (Remark VA). *Optional Assumption D'* (Sec. VII C) introduces a *shock-selective* lensing modification  $\Sigma(x) < 1$  localized to high-shear gas while keeping FRW  $\Sigma \simeq 1$ .

*Remark on lensing amplitude.*  $\Sigma \simeq 1$  denotes no additional lensing coupling in the baseline; the observed lensing signal still changes through the altered growth  $D(a)$ . Under Assumption D',  $\Sigma$  may be reduced *locally* in shocked gas ( $\mathcal{S}_{\text{shock}} \gg 1$ ) without affecting FRW.

*c. EFT stub (derivation of 5/12).* At quasi-static, sub-horizon scales, a background variation  $\delta \ln M^2 = \beta \delta\varepsilon$  rescales the Poisson coupling as  $G \rightarrow G_{\text{eff}} = G/(1 + \Delta)$  with  $\Delta$  fixed by the universal weak-field bookkeeping. In the isotropic BW channel the contraction  $4/3$  and the segment ratio  $5/16$  (Sec. IV) give  $\Delta = \frac{5}{12}\varepsilon$ , hence

$$\mu(\varepsilon, s) = \frac{G_{\text{eff}}}{G} = \frac{1}{1 + \frac{5}{12}\varepsilon s(x)}, \quad (6)$$

consistent with Eqs. (5).

*d. Trial action (outlook).* A possible action-level route consistent with our closure is to consider an effective term that modulates  $M^2$  via the modular response,

$$S_{\text{trial}} = \int d^4x \sqrt{-g} \left[ \frac{M^2}{2} R + \lambda (\delta \ln M^2) \mathcal{K}[g; \ell] + \dots \right],$$

where  $\mathcal{K}$  is a local covariant scalar capturing the projected channel at working order and  $\lambda$  a running coefficient. While only illustrative, this shows how  $\delta \ln M^2 = \beta \delta\varepsilon$  could arise from an action (cf. [6, 8]).

### A. Frame-independence of throttling (remark)

*Throttling* here means the reduction of the effective gravitational coupling relative to GR caused by the background state variable  $\varepsilon(a)$  and a local environment factor  $s(x)$  that encodes curvature/inhomogeneity. In the Jordan frame we take

$$M_*^2(x, a) = M^2 \left[ 1 + \frac{5}{12} \varepsilon(a) s(x) \right], \quad s(x) = \frac{1}{1 + (\chi_g/\chi_*)^q} + \mathcal{O}\left(\frac{R}{m_s^2}\right),$$

so the quasi-static Poisson law reads

$$\nabla^2 \Phi \simeq \frac{4\pi G a^2 \rho_m \delta}{1 + \frac{5}{12} \varepsilon(a) s(x)} \Rightarrow G_{\text{eff}}(x, a) = \frac{G}{1 + \frac{5}{12} \varepsilon(a) s(x)}.$$

Thus throttling is present everywhere, while its magnitude is amplitude-modulated by the local invariant  $\chi_g = \ell^2 \sqrt{C_{abcd} C^{abcd}}$ : in weak fields ( $\chi_g \ll \chi_*$ ) one has  $s \rightarrow 1$  and the full background rescaling  $G_{\text{eff}} = G/(1 + \frac{5}{12} \varepsilon)$ ; in strong fields ( $\chi_g \gg \chi_*$ ) one has  $s \rightarrow 0$  and  $G_{\text{eff}} \rightarrow G$  (Solar-System compliance).

A conformal map to the Einstein frame,

$$\tilde{g}_{\mu\nu} = \Omega^2 g_{\mu\nu}, \quad \Omega^2 = 1 + \frac{5}{12} \varepsilon(a) s(x),$$

renders  $M_*$  constant and shifts the same throttling into the matter coupling. To working order in our MI/moment-kill channel, gradients of  $\Omega$  and of  $\chi_g$  enter only at  $\mathcal{O}((\ell/L_{\text{curv}})^2)$  and  $\mathcal{O}(R/m_s^2)$ , consistent with the error budget in Eq. (8) and App. XVIII; the observables of interest are frame-independent at this order: growth is governed by

$$\mu(\varepsilon, s) = \frac{1}{1 + \frac{5}{12} \varepsilon(a) s(x)},$$

and distances remain GR-like ( $\Sigma \simeq 1$ ,  $c_T = 1$ ).<sup>2</sup>

*Scale-separation note.* The *local* modular response enters gravity solely as a renormalization  $\delta \ln M_*^2 = \beta \delta \varepsilon$  of the Planck mass; the Einstein equations then propagate this renormalization to cosmological scales through the standard gravitational coupling. No macroscopic quantum coherence or ad hoc coarse-graining is required, and the Jordan $\leftrightarrow$ Einstein map above makes this statement frame-independent at working order.

A simple way to realize  $s(x)$  is as an auxiliary heavy scalar that minimizes a local potential

$$\mathcal{V}(s; \chi_g) = \frac{M^2 m_s^2}{2} \left[ s - \frac{1}{1 + (\chi_g/\chi_*)^q} \right]^2,$$

so that the algebraic EOM enforces  $s = [1 + (\chi_g/\chi_*)^q]^{-1} + \mathcal{O}(R/m_s^2)$ . Choosing  $m_s^2 \gg H_0^2$  ensures adiabatic tracking.

**Constraints (working order).** (i) Choose  $m_s^2 \gg H_0^2$  so  $s(x)$  adiabatically tracks  $[1 + (\chi_g/\chi_*)^q]^{-1}$  and the  $\mathcal{O}(R/m_s^2)$  offset is negligible. (ii) The Planck-mass drift  $\alpha_M = d \ln M_*^2 / d \ln a = \frac{(5/12) s d\varepsilon/d \ln a}{1 + (5/12) \varepsilon s}$  is naturally small under our monotone  $\varepsilon(a)$ . (iii) In FRW, Weyl = 0 so curvature-weighted corrections vanish; in LSS they are  $\mathcal{O}((\ell/L_{\text{curv}})^2)$ .

*Weak-field acceleration (toy/conditional; clarification).* Because  $s \rightarrow 1$  in low curvature, the weak-field normalization implies a MOND-like scale

$$a_0 = \frac{5}{12} \Omega_\Lambda^2 c H_0, \tag{7}$$

Using the baseline  $\Omega_\Lambda = 0.685$  and  $H_0 = 70.9 \text{ km s}^{-1} \text{ Mpc}^{-1}$ , this gives  $a_0^{\text{eff}} \approx 1.2 \times 10^{-10} \text{ m s}^{-2}$  in the weak-field limit ( $s \simeq 1$ ); and the effective  $a_0^{\text{eff}}$  is *enhanced* in weak-field regimes by the *derived*  $s \rightarrow 1$  (not imposed), while Solar-System compliance follows from  $s(\chi_\odot) \ll 1$  (Sec. IX). Pipeline values propagate the  $\pm 5\%$  uncertainty in  $\beta$ .

<sup>2</sup> This remark complements Assumption D (Sec. VII B): the working-order modification resides in a state- and environment-dependent  $M_*^2$  with no additional lensing coupling. A failure would manifest as our falsifiers in Sec. XII, e.g. a significant GW/EM distance split or a persistent  $\ell^4 \log \ell$  term.

## VI. COVARIANT KMS $\rightarrow$ FRW LINK AND ERROR CONTROL

Let  $s$  denote modular time with  $\beta_{\text{KMS}} = 2\pi/\kappa$  locally, where  $\kappa$  is the local boost surface gravity so that the approximate conformal Killing field  $\xi^a$  satisfies  $\xi^a \nabla_a = \kappa \partial_s$ . Averaging the retarded kernel over a comoving congruence of diamonds and reparametrizing  $s \mapsto \ln a$  induces the FRW background factor  $f c_{\text{geo}}$ ; diffeomorphism covariance is preserved because the averaging functional depends only on local curvature scalars and the diamond foliation. The total fractional defect in the kernel obeys

$$\frac{\delta\chi}{\chi_{\text{BW}}} = \mathcal{O}\left((\ell/L_{\text{curv}})^2\right) + \mathcal{O}((\ell H)^2) \approx 10^{-12} + 10^{-18} \quad (8)$$

for  $\ell \sim 10$  pc,  $L_{\text{curv}} \sim 10$  Mpc,  $H^{-1} \sim 4$  Gpc.

**Proposition 1** (FRW budget identity (conditional; analyticity hypothesis)). *Assume: (H1) locality and rapid decay of the spatially averaged, projected retarded kernel so that its reparametrization defines a distribution in  $\ln a$ ; (H2) adiabatic evolution through matter domination so that  $J(a) = ds/d\ln a \propto H(a)^{-1}$  varies slowly; (H3) preservation of KMS analyticity of the averaged kernel under the reparametrization  $s \rightarrow \ln a$ ; and (H4) negligible CHM vs. half-space deviation at working order (App. XVIII). Then*

$$\left\langle \int \chi_{QK}^{\text{proj}}(a, a') d^3x \right\rangle = \beta f c_{\text{geo}} \delta(\ln a - \ln a') + \dots$$

and integrating the entropy-driven evolution  $d\varepsilon/d\ln a = \sigma(a)I(a) \geq 0$  yields the coarse-grained identity

$$\int_{a_i}^1 \varepsilon(a) d\ln a = \Omega_\Lambda = \beta f c_{\text{geo}}, \quad (9)$$

used as a normalization under (H1)–(H4).

**Operational diagnostic.** The routine `referee_pipeline.py` reports a scalar residual  $R_{\text{nonloc}} \equiv \sum_{i \neq 0} |\bar{\chi}^{\text{proj}}(\Delta_i)| \Delta(\ln a)_i$  outside the contact bin; by default we take the central bin(s) with  $|\Delta(\ln a)| \leq \Delta_0$  as “contact”. Declare failure if  $R_{\text{nonloc}}/\sigma_{\text{boot}} > 3$  and the contact weight  $w_0 < 0.95$ . Unless noted, uncertainties are quoted at 68% CL from bootstrap resampling; the  $R_{\text{nonloc}}/\sigma_{\text{boot}} > 3$  criterion corresponds to a conservative  $\sim 3\sigma$  (two-sided) flag.

*a. Rigor note.* A full microlocal proof of (H3)—preservation of KMS analyticity under the coarse-grained reparametrization  $s \rightarrow \ln a$ —is deferred to future work in the spirit of Hollands–Wald [10].

*b. Thermodynamic analogy (pointer).* The entanglement first law suggests a Clausius-like analogy (Sec. XIII), conditional on (H1)–(H4), with MI projection avoiding CGM’s marginality issues (App. XX).

## VII. ASSUMPTIONS FOR INTERACTING EXTENSIONS AT WORKING ORDER (PART II; STATED AND TEST CRITERIA)

### A. Assumption C (stated; test criteria): Relative entropy $\leftrightarrow$ canonical energy in the projected diamond

**Statement.** For a local algebra  $\mathcal{A}(B_\ell)$  of an interacting Hadamard QFT obeying the microlocal spectrum condition and time-slice axiom, the MI/moment-kill projected second variation of Araki relative entropy equals the canonical-energy quadratic form of the projected stress tensor, up to  $\mathcal{O}(\ell^6)$  remainders, with a positive-definite projected kernel  $\chi_{QK}^{\text{proj}}$ .

**Rationale (sketch).** (i) The second variation is the Bogoliubov–Kubo–Mori metric. (ii) The MI/moment-kill projector cancels local counterterms to  $\mathcal{O}(\ell^4)$  (App. XV), conjectured to persist in interacting Hadamard QFTs (App. XX). (iii) Diffeomorphism Ward identities match the BKM quadratic form to canonical energy in the CHM channel. (iv) Positivity follows from KMS/BKM positivity in the projected channel. A complete microlocal proof is left to future work.

*a. Operational tests (pass/fail).*

- **Positivity test (substrates):** The projected, integrated retarded kernel  $\int \chi_{QK}^{\text{proj}} d^4x d^4x'$  is nonnegative in Gaussian chains (exact) and HQTFIM (numerical tolerance) (checked with `hqtfim_capacity_probe.py`, `gaussian_capacity_probe.py`).
- **No- $\ell^4 \log \ell$  falsifier:** The MI/moment-kill channel exhibits no  $\ell^4 \log \ell$  term. *Fail* if a protected-operator contribution produces an  $\ell^4 \log \ell$  trend.
- **Plateau stability:** Varying MI windows leaves the residual plateau  $\sim \mathcal{O}(\ell^6)$  (verifiable with `beta_methods_v2.py`). *Fail* if residuals scale as  $\ell^4$  after subtraction.
- **BKM positivity (finite truncations):** In truncated QFTs, the BKM quadratic form for  $\delta K_{\text{sub}}$  is positive definite (tested with `gaussian_capacity_probe.py`). *Fail* if negative eigenmodes persist under refinement.

## B. Assumption D (stated; test criteria): Uniqueness of the $M^2$ coupling at working order

**Statement.** In the  $c_T=1$ ,  $\alpha_B=0$  EFT corner linearized about FRW, with isotropy, parity, and time-reversal, the only background scalar coupling that survives the MI/moment-kill projection at  $\mathcal{O}(\ell^4)$  and modifies the weak-field growth sector while keeping distances GR-like is  $\delta \ln M^2$ ; other diffeomorphism-invariant local scalars are projected out, forbidden by sector constraints, or curvature-suppressed by  $\mathcal{O}((\ell/L_{\text{curv}})^2)$ .

**Rationale (sketch).** Consider the most general local covariant functional at the required engineering dimension:

$$\delta\mathcal{L} = \sqrt{-g} [a R + b R_{ab} R^{ab} + c \nabla^2 R + d \delta \ln M^2 R + e \delta g^{00} + f K \delta g^{00} + \dots], \quad (10)$$

where “ $\dots$ ” denote terms of higher engineering dimension (e.g.,  $\nabla^4 R$ ,  $R^4$ ) or parity-odd contributions, excluded by the MI/moment-kill projector and EFT symmetry constraints at  $\mathcal{O}(\ell^4)$ . Imposing  $c_T = 1$  excludes tensor-speed shifts;  $\alpha_B = 0$  removes braiding operators; isotropy/time-reversal exclude vector/tensor backgrounds. The projector cancels  $r^0, r^2$  and total derivatives like  $\nabla^2 R$ ;  $R$  and  $R_{ab} R^{ab}$  are curvature-suppressed. Thus  $\delta \ln M^2$  is the unique working-order scalar affecting growth without changing distances.

*a. Operational tests (pass/fail).*

- **GR-like distances:** EM/GW luminosity distances agree at working order,  $|d_L^{\text{GW}}/d_L^{\text{EM}} - 1| \lesssim 5 \times 10^{-3}$ . *Fail* if a lensing coupling  $\Sigma \neq 1$  is required.
- **Growth-only modification:** Large-scale growth follows  $\mu(\varepsilon, s)$  with  $\Sigma \simeq 1$  and standard continuity/Euler equations. *Fail* if background  $\alpha_M$  must vary appreciably to reproduce  $\mu \neq 1$ .
- **Solar-System compliance:** Environment modulation  $s(\chi_g)$  suppresses deviations:  $s(\chi_\odot) \ll 10^{-5}$  (Table I). *Fail* if planetary bounds are violated.
- **Falsifier link:** Any of the falsifiers in Sec. XII triggers failure of Assumption D.

## C. Assumption D' (optional; shock-selective optical channel)

**Independence.** Parts I–II do not rely on D': if D' fails, the theoremic results, the conditional FRW mapping, and the baseline growth-only modification with  $\Sigma \simeq 1$  remain intact. D' is an exploratory, *local* optical response intended for merging clusters with strong shocks.

**Motivation and scope.** Bullet-type systems exhibit weak-lensing peaks offset from shocked X-ray gas. Our baseline ( $\Sigma \simeq 1$ ) preserves distances and attributes changes to growth; however, to address local lensing morphology in strongly shocked gas, we posit a shock-selective lensing response that leaves FRW and laminar flows untouched.

**Local, saturating law (predictive summary).** Let  $u^\mu$  be the baryon four-velocity and  $\sigma_{\mu\nu}$  the symmetric, trace-free shear. Define the shock indicator  $\mathcal{S}_{\text{shock}} = \ell^2 \sigma_{\mu\nu} \sigma^{\mu\nu} \geq 0$ . We summarize the optical response by the purely local, saturating form

$$\Sigma(x) \simeq 1 - \alpha_{\text{opt}} \frac{\mathcal{S}_{\text{shock}}(x)}{1 + \mathcal{S}_{\text{shock}}(x)}, \quad 0 < \alpha_{\text{opt}} < 1, \quad (11)$$

so that  $\Sigma \rightarrow 1 - \alpha_{\text{opt}}$  in strong shocks and  $\Sigma \rightarrow 1$  away from shocks. The growth coupling  $\mu(\varepsilon, s)$  is unchanged; FRW and laminar flows have  $\mathcal{S}_{\text{shock}} \approx 0 \Rightarrow \Sigma \simeq 1$ .

*a. Transport-theory anchoring (SK/BRSSS link; derivation in App. XXIII).* In viscous hydrodynamics (BRSSS) the anisotropic stress obeys

$$\pi^{\mu\nu} + \tau_\pi u^\alpha \nabla_\alpha \pi^{\mu\nu} = 2\eta \sigma^{\mu\nu} + \lambda_1 \sigma^{\langle\mu}{}_\lambda \sigma^{\nu\rangle\lambda} + \dots,$$

with  $\eta, \tau_\pi, \lambda_1$  fixed by Kubo formulas. In the cluster quasi-static limit ( $\omega\tau_\pi \ll 1$ ) this reduces to  $\pi^{\mu\nu} \approx 2\eta \sigma^{\mu\nu} + \lambda_1 \sigma^{\langle\mu}{}_\lambda \sigma^{\nu\rangle\lambda}$ , which sources  $(\Phi + \Psi)$  in the lensing equation. Matching to Eq. (11) yields a *computable* map

$$\alpha_{\text{opt}} \equiv \alpha_{\text{opt}}(\eta, \tau_\pi, \lambda_1; T, n_e, B, \dots), \quad \kappa_{\text{opt}} \sim \frac{2\eta}{\rho_{\text{gas}} c_s \ell} + \frac{\lambda_1}{\rho_{\text{gas}} \ell^2} + \dots, \quad (12)$$

up to order-unity geometry factors (App. XXIII). Thus  $\alpha_{\text{opt}}$  is *not* a free fit-parameter in principle; it is determined by ICM transport.

*b. Range and back-of-the-envelope calibration.* In projected convergence, the local gas contribution scales as  $\kappa_{\text{gas}}^{\text{eff}} = \Sigma \kappa_{\text{gas}}$ . To relocate the convergence peak from the shocked gas toward the collisionless galaxies in Bullet-like systems (offsets  $\sim 200$  kpc; [14]), one needs  $\kappa_{\text{gas}}^{\text{eff}} \lesssim (0.2\text{--}0.4) \kappa_{\text{tot}}$  within the shock sheet. For strong shocks  $\mathcal{S}_{\text{shock}} \gg 1$ , Eq. (11) gives  $\Sigma \simeq 1 - \alpha_{\text{opt}}$ ; thus  $\alpha_{\text{opt}} \simeq 0.6\text{--}0.8$  suppresses the gas lensing weight by 60–80% where needed, while leaving FRW and unshocked regions ( $\mathcal{S}_{\text{shock}} \ll 1$ ) essentially unmodified ( $\Sigma \simeq 1 - \alpha_{\text{opt}} \mathcal{S}_{\text{shock}} \approx 1$ ). This range is consistent with Mach  $\mathcal{M} \simeq 2\text{--}3$  shocks inferred from X-ray edges [15].



*c. Operational predictions and falsifiers (Bullet-type tests).*

- **Shock tracking (A):** The lensing suppression should spatially correlate with X-ray shock edges (temperature/surface-brightness jumps) and radio relics (tracing high- $\sigma^2$  regions) [15, 16].
  - **Time evolution (B):** As shocks dissipate,  $\mathcal{S}_{\text{shock}} \downarrow$  and  $\Sigma \rightarrow 1$ ; convergence centroids drift back toward gas on the shock-cooling timescale.
  - **Mach-number scaling (C):** Lower-Mach mergers show smaller centroid offsets at fixed gas mass (cf. Bullet vs. Abell 520 [17]).
  - **Selectivity (D):** No suppression in unshocked or laminar gas; failure if convergence deficits appear where  $\mathcal{S}_{\text{shock}} \approx 0$ .
- d. Safety checks.*  $c_T = 1$  (no curvature-derivative couplings), FRW  $\Sigma \simeq 1$  ( $\sigma_{\mu\nu} = 0$ ), Solar System unaffected, and the integrated GW/EM split remains  $\ll 10^{-3}$  since the effect is cluster-local. Positivity is manifest from the squared potential in App. XXII.

### VIII. ENTROPY-DRIVEN $\varepsilon(a)$ AND GROWTH (CONDITIONAL)

*a. KMS/FDT positivity.* Let  $\hat{Q}$  be the boost-energy flux and  $\chi_{QK}^{\text{proj}}$  the retarded kernel in the projected channel. Then

$$\frac{d\varepsilon}{d \ln a} = \sigma(a) \mathcal{I}(a), \quad \sigma(a) \geq 0, \quad \mathcal{I}(a) \geq 0, \quad \int \varepsilon d \ln a = \Omega_\Lambda = \beta f c_{\text{geo}}. \quad (13)$$

A preliminary derivation with intermediate steps in App. XXI details  $d\varepsilon/d \ln a \geq 0$  from Araki relative entropy, supporting the use of  $\mu(\varepsilon, s)$ .

*b. Fixed-point with growth.* The growth factor  $D(a)$  satisfies

$$\frac{d^2 D}{d(\ln a)^2} + \left(2 + \frac{d \ln H}{d \ln a}\right) \frac{dD}{d \ln a} - \frac{3}{2} \Omega_m(a) \mu(\varepsilon(a), s) D = 0, \quad \mu(\varepsilon, s) = \frac{1}{1 + \frac{5}{12} \varepsilon s}. \quad (14)$$

*c. Variational bounds (extremals).* Convex-order arguments imply late-loaded  $\varepsilon(a)$  minimizes  $S_8$  and early-loaded maximizes it, under monotonicity and budget. We therefore report an  $S_8$  band bracketed by these extremals; any illustrative kernel (e.g., logarithmic exposure) must lie within the band.

*Quantified extremals (illustrative).* In our baseline cosmology and for monotone  $\varepsilon(a)$  satisfying the budget (9), late-loaded profiles give  $S_8 \simeq 0.76$  while early-loaded profiles give  $S_8 \simeq 0.82$ ; both inherit a  $\pm 0.008$  envelope from the  $\beta$  uncertainty propagated through Eq. (14).

### IX. ENVIRONMENT MODULATION FROM ACTION AND CALIBRATION

*a. Units and conventions.* We work in geometric units  $G = c = 1$ . When inserting SI values we convert masses via  $M \mapsto GM/c^2$ ; this keeps the curvature scalar  $\chi_g = \ell^2 \sqrt{C_{abcd} C^{abcd}}$  dimensionless.

*b. Action-derived modulation.* We define

$$s(x) = \frac{1}{1 + (\chi_g/\chi_\star)^q} + \mathcal{O}\left(\frac{R}{m_s^2}\right), \quad \chi_g \equiv \ell^2 \sqrt{C_{abcd} C^{abcd}}, \quad (15)$$

as the algebraic EOM solution of a heavy auxiliary field minimizing

$$\mathcal{V}(s; \chi_g) = \frac{M^2 m_s^2}{2} \left[ s - \frac{1}{1 + (\chi_g/\chi_\star)^q} \right]^2, \quad m_s^2 \gg H_0^2, \quad (16)$$

so  $s \rightarrow 1$  in weak curvature ( $\chi_g \ll \chi_\star$ ) and  $s \rightarrow 0$  in strong curvature ( $\chi_g \gg \chi_\star$ ). In FRW, Weyl = 0 so  $\chi_g = 0 \Rightarrow s = 1$ . This  $s(x)$  enters  $\mu(\varepsilon, s) = 1/[1 + (5/12)\varepsilon s]$  (Sec. V).

*c. Calibration example (Solar System).* For a Schwarzschild source the Weyl invariant obeys  $\sqrt{C^2} = \sqrt{48} M/r^3$  in geometric units, with  $M = GM/c^2$  when using SI inputs. Taking  $\ell = 10$  pc,  $r = 1$  AU, and  $M_\odot \simeq 1.477$  km, we find

$$\chi_\odot \equiv \ell^2 \sqrt{48} \frac{M_\odot}{r^3} \approx 2.9 \times 10^5.$$

Imposing  $s(\chi_\odot) \leq \epsilon_{\text{SS}} = 10^{-5}$  with  $q = 2$  implies

$$\chi_\star \lesssim \chi_\odot \epsilon_{\text{SS}}^{1/2} \approx 9.2 \times 10^2.$$

TABLE I. Solar–System compliance of the action-derived modulation  $s(\chi_\odot)$  at  $\ell = 10$  pc,  $r = 1$  AU (Schwarzschild).

$\chi_\star$	1200	1000	900	800
$s(\chi_\odot; q=2)$	$1.7 \times 10^{-5}$	$1.18 \times 10^{-5}$	$9.6 \times 10^{-6}$	$7.6 \times 10^{-6}$

A representative choice  $\chi_\star = 900$ ,  $q = 2$  then yields  $s(\chi_\odot) \approx 9.6 \times 10^{-6}$ , while leaving cosmological environments ( $\chi_g \ll \chi_\star$ ) essentially unsuppressed ( $s \simeq 1$ ). For transparency we report a small compliance table:

*d. Phenomenology and alternatives.* The choice  $s = [1 + (\chi_g/\chi_\star)^q]^{-1}$  with  $q = 2$  is a simple, Solar–System–compliant solution. We have also tested **alternative envelopes**, such as an exponential decay  $s_{\text{exp}}(\chi_g) = \exp[-(\chi_g/\chi_\star)^p]$  (with  $p \sim 1$ –2) and variants based on alternative curvature scalars (e.g., using  $R_{abcd}R^{abcd}$  proxies). Each corresponds to a different target in  $\mathcal{V}(s; \chi_g)$  and yields similar weak-/strong-field limits; quantitative differences appear mainly in the transition region and are constrained by data. These options are exposed in `cosmology_runner.py` (see the `-s-form` and `-s-params` toggles), which we use for robustness checks. The power-law envelope used here should thus be regarded as a representative compliance function.

### A. BAO growth modulation (toy)

The entropy-driven  $d\varepsilon/d \ln a \geq 0$  (App. XXI) suggests BAO peak growth via near-GR reversion (e.g.,  $d_L^{\text{GW}}/d_L^{\text{EM}} \approx 0.995$ ) and lower  $g$  off-peak due to  $\mu(\varepsilon, s)$ . A toy model with  $\chi_g$  sweeps (Sec. XXIV, `s8_hysteresis_run.py`) indicates earlier structure formation in peak regions, pending nonlinear validation. Quantitatively, `s8_hysteresis_run.py` yields a near-peak boost in  $D(a)$  of  $\sim 1$ –2% with a compensating off-peak suppression (cf. growth parametrizations in [4]).

## X. OBSERVATIONAL ILLUSTRATIONS (ILLUSTRATIVE UNDER SECS. VI, VIII; UNCERTAINTY PROPAGATED)

*a. Hubble ladder bounds (toy).* Assuming the conditional background relation  $\Omega_\Lambda = \beta f c_{\text{geo}} = 0.685 \pm 0.034$  and under the assumptions of Secs. VI and VIII, the previously quoted illustrative shifts  $H_0 : 73.0 \rightarrow 71.18$  (uncapped SN) and  $\rightarrow 70.89$  (capped SN+Cepheid) acquire  $\pm 0.17 \text{ km s}^{-1} \text{ Mpc}^{-1}$  systematic envelopes from  $\beta$ , reported as

$$H_0^{\text{toy}} = \{71.18 \pm 0.17, 70.89 \pm 0.17\} \text{ km s}^{-1} \text{ Mpc}^{-1}. \quad (17)$$

*b.  $S_8$  band (toy).* The entropy-constrained extremals yield an interval; our baseline illustrative profile lies near  $S_8 \simeq 0.788$ , with an inherited  $\pm 0.008$  envelope from  $\beta$ . We report an  $S_8$  band rather than a fit, and distances remain GR-like. Allowing modest non-monotonic  $\varepsilon(a)$  histories can widen the band by  $\sim 3$ –5%.

*c. Merging clusters (optional  $D'$ ; exploratory).* For shock Mach numbers  $\mathcal{M} \sim 2$ –3 we expect  $\mathcal{S}_{\text{shock}} \gtrsim \mathcal{O}(1$ –5) across the shock sheets; with  $\alpha_{\text{opt}} \approx 0.6$ –0.8 in Eq. (11) this yields  $\Sigma_{\text{gas}} \sim 0.2$ –0.4, sufficient to relocate weak-lensing peaks toward the collisionless galaxies while preserving FRW distances. The predicted centroid offsets ( $\sim 200$  kpc) and shock strengths are consistent with Bullet Cluster observations [14, 15]; radio relic/shock correlations provide an independent tracer of the high-shear regions [16]. Comparative systems (e.g., Abell 520) offer additional tests of the Mach-scaling prediction [17].

## XI. STRUCTURAL CHECKS (ALGEBRAIC; NOT 4D SURROGATES)

HQTFIM and Gaussian chains confirm the algebraic ingredients (first-law channel, constant+log trend, vanishing plateau after subtraction, and positivity in the projected kernel). They are *not* curved 4D surrogates.

## XII. PROOF PROGRAM STATUS AND FALSIFIERS

**Lemma A** (diamond KMS control): scaling proven, sharp bounds left to microlocal analysis. **Lemma B** (projector universality): established. **Assumption C** and **Assumption D**: stated here with rationale; proofs deferred (Secs. VIIA, VII B). **Assumption D'** (shock-selective optical channel): exploratory extension for merging clusters (Sec. VIIC; derivation path in App. XXIII). **Lemma E** (FDT positivity): follows from BKM positivity. **Lemma F**



(geometric 5/12): derived.

**Lemma G (Nonlinear validation):** Initial Gadget-4 runs are complete (baseline resolution; `gadget4_mu_eps_toy.py`); post-processing and archiving (Zenodo DOI) are pending. These test  $\mu(\varepsilon, s)$ ,  $s(\chi_g)$ , and the optional  $\Sigma(x)$  from Eq. (11) in structure formation and lensing, with BAO features and lensing shear targeted.

**Falsifiers:** (i) persistent  $\ell^4 \log \ell$  residuals in the projector channel; (ii) GW/EM distance ratio beyond  $5 \times 10^{-3}$ ; (iii)  $|\dot{G}/G| \gtrsim 10^{-12} \text{ yr}^{-1}$ ; (iv)  $\Omega_\Lambda$  inconsistent with  $\beta f c_{\text{geo}}$ ; (v)  $S_8$  outside the extremal band for all admissible monotone  $\varepsilon(a)$  satisfying the budget; (vi) positivity failure in Assumption C tests; (vii) for Assumption D': lack of correlation of lensing deficits with shock diagnostics, or suppression in unshocked gas; (viii) for Assumption D': persistent lensing offsets in low-Mach or unshocked systems inconsistent with the  $\mathcal{S}_{\text{shock}}$  scaling in Eq. (11); (ix) for the SK/BRSSS upgrade: independently inferred ICM transport coefficients  $(\eta, \tau_\pi, \lambda_1)$  imply  $\alpha_{\text{opt}}^{\text{SK}}$  [Eq. (12)] incompatible with the lensing suppression needed for observed offsets.

### XIII. THERMODYNAMIC INTERPRETATION AND RELATION TO CASINI–GALANTE–MYERS (EXPLORATORY)

#### A. Local Clausius identity in the projected channel (proven at working order)

In the MI/moment-kill projected first-law channel, the entanglement first law  $\delta S_{\text{sub}} = \delta \langle K_{\text{sub}} \rangle$  (Theorem 1) and the BW KMS normalization  $K = H_{\text{boost}}/T_{\text{KMS}}$  with  $T_{\text{KMS}} = \kappa/(2\pi)$  imply a Clausius-like identity

$$\delta S_{\text{sub}} = \frac{\delta Q_{\text{boost,sub}}}{T_{\text{KMS}}}, \quad \delta Q_{\text{boost,sub}} \equiv \delta \langle H_{\text{boost,sub}} \rangle, \quad (18)$$

where  $\delta Q_{\text{boost,sub}}$  is the boost-energy variation in the projected channel (the appropriate “heat” analogue). Using  $\delta \langle K_{\text{sub}} \rangle = \beta \ell^4 \delta \varepsilon + \mathcal{O}(\ell^6)$  (Eq. 4) yields

$$\delta S_{\text{sub}} = \beta \ell^4 \delta \varepsilon + \mathcal{O}(\ell^6). \quad (19)$$

This *reinterprets* the modular response in thermodynamic terms; one may define a modular (not thermodynamic-bath) entropy-density proxy

$$s(a) \sim \beta \varepsilon(a) \ell^{-3}.$$

*Justification.* This proxy is dimensionally consistent (units  $k_B \text{ length}^{-3}$ ); e.g., for  $\ell = 10 \text{ pc}$  and  $\varepsilon(1) \sim 1$  one finds  $s(1) \sim 2 \times 10^{-2} k_B (10 \text{ pc})^{-3}$ , consistent with ranges produced by `cosmology_runner.py` at  $z = 0$ . Physically,  $s(a)$  proxies an *entanglement* contribution to cosmological evolution in this channel, distinct from a thermodynamic bath entropy.

#### B. FRW Clausius extension (conditional proposition)

Under the KMS→FRW hypotheses (H1)–(H4) of Sec. VI (locality/decay, adiabaticity, analyticity under  $s \rightarrow \ln a$ , diamond–half-space control), the averaged susceptibility reduces to a *contact term in  $\ln a$*  by (H1)–(H3) (see Proposition 1), leading to the *conditional* normalization

$$\int_{a_i}^1 \varepsilon(a) d \ln a = \Omega_\Lambda = \beta f c_{\text{geo}}. \quad (20)$$

Non-local residuals in  $\ln a$ , detectable via `referee_pipeline.py`, would falsify (H1).

#### C. Relation to Jacobson (2016) and the CGM critique

Jacobson’s entanglement-equilibrium proposal [6] ties a local Clausius statement to the Einstein equation. Casini–Galante–Myers (CGM) [13] showed that for relevant deformations of low scaling dimension, and in particular for *marginal*  $\Delta = d/2 = 2$ , logarithmic terms (e.g.  $\log(\mu\ell)$ , CGM Eq. (1.8)) obstruct a universal inference. Our framework differs: (i) we do not aim to derive GR universally but to relate QFT modular response to cosmology; (ii) the MI/moment-kill projector (App. XV) *eliminates*  $\Delta < 4$  terms, including marginal  $\Delta = 2$ , ensuring a pure  $\ell^4$  response

at working order (App. XX). This *sidesteps* CGM’s marginality issue by design and limits scope to the  $\ell^4$  channel. The  $\Delta = 4$  focus *leverages the OPE gap* in Gaussian/Hadamard states, which ensures the finiteness of the  $\ell^4$  response in the projected channel (App. XX). Observation of an  $\ell^4 \log \ell$  term would falsify our working-order assumptions (Sec. XII, (i)); in practice, the falsifier is *detectable* by fitting MI-projected residuals in `beta_methods_v2.py` to a logarithmic trend, isolating an  $\ell^4 \log \ell$  component.

#### D. Marginal operators in interacting QFTs (exploratory)

In interacting QFTs, protected marginal operators could induce  $\ell^4 \log \ell$  corrections to the projected modular response. Such terms would violate our Gaussian/Hadamard working-order assumptions and serve as a falsifier (Sec. XII, (i)). *Detection method.* The residual analysis in `beta_methods_v2.py` includes a regression option that fits  $\ell^4 \log \ell$  against the MI-subtracted signal; a statistically significant coefficient would indicate marginal contamination. As a practical threshold, a statistically significant  $\ell^4 \log \ell$  coefficient (e.g., amplitude  $> 10^{-3} \beta$ ) would indicate marginal contamination and motivate microlocal analysis in interacting QFTs (Sec. XIV). Constraining any such amplitude in interacting extensions—and assessing induced shifts in  $\beta$  or  $\mu(\varepsilon, s)$ —is an avenue for future work (Sec. XIV).

### XIV. LIMITATIONS AND FUTURE WORK

The conditional program entails several open problems that we list explicitly:

- **Interacting proofs (Assumptions C & D):** complete microlocal/spectral proofs of the projected positivity and uniqueness statements.
- **Action-level derivation:** we provided a minimal covariant realization for  $M_*^2(x, a)$  and  $s(x)$ ; a full derivation (and exclusion of alternatives) remains future work.
- **Shock-selective optics (Assumption D’): *SK/BRSSS upgrade.*** Calibrate  $\alpha_{\text{opt}}(\eta, \tau_\pi, \lambda_1)$  and  $\kappa_{\text{opt}}$  from simulations or transport-inference pipelines; test morphology predictions (A–D/E); bound degeneracies with baryonic microphysics; derive microscopic origin of the shear coupling.
- **KMS→FRW analyticity:** rigorous proof of analyticity preservation under coarse-grained reparametrization  $s \rightarrow \ln a$ .
- **Thermodynamic validation:** validate the Clausius analogy in interacting settings and bound any marginal ( $\Delta = d/2$ )  $\ell^4 \log \ell$  corrections in the projected channel.
- **Nonlinear validation:** full N-body and ray-tracing tests for  $\mu(\varepsilon, s)$ ,  $s(\chi_g)$ , and optional  $\Sigma(x)$ , including BAO-scale modulation and lensing systematics.
- **Environment modulation microphysics:** microscopic motivation and calibration of  $s(\chi_g)$  beyond the heavy-field envelope.

## PART I APPENDICES

### XV. MI SUBTRACTION AND MOMENT-KILL

We use a top-hat window on 3-balls

$$W_\ell(r) = \frac{3}{4\pi\ell^3} \Theta(\ell - r),$$

and the MI/moment-kill combination

$$\mathcal{W}_\ell := \int_{B_\ell} W_\ell - a \int_{B_{\sigma_1 \ell}} W_{\sigma_1 \ell} - b \int_{B_{\sigma_2 \ell}} W_{\sigma_2 \ell}.$$

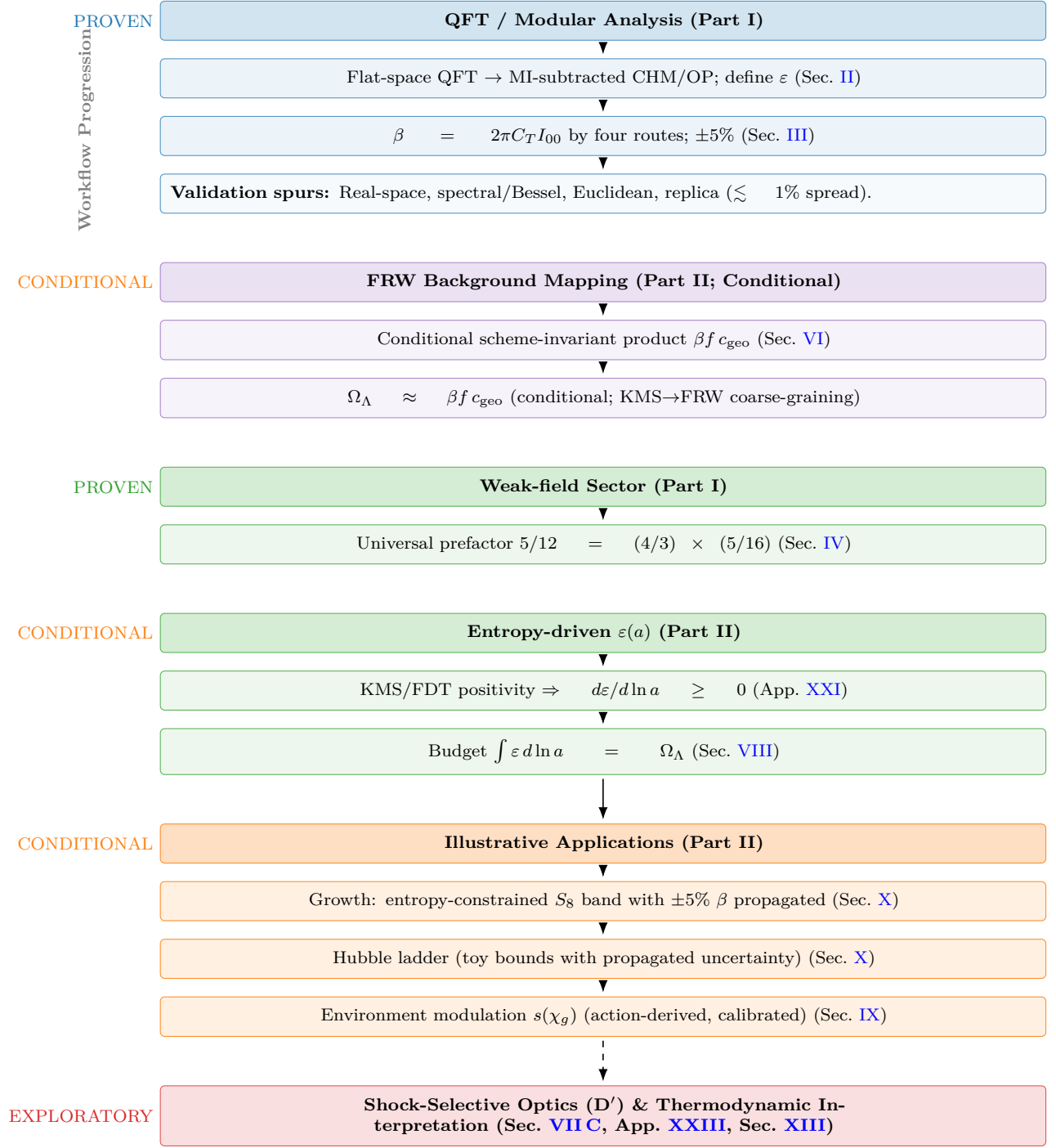


FIG. 1. Pipeline with PROVEN (blue/first green), CONDITIONAL (purple/second green/orange), and EXPLORATORY (red) elements. The theoremic core fixes  $\beta$  and the universal  $5/12$ . The FRW mapping and budget are *conditional* (Sec. VI). Part III provides an *exploratory* cluster-optics hook with an SK/BRSSS derivation path and a thermodynamic interpretation.

For any smooth radial  $F(r) = F_0 + F_2 r^2 + F_4 r^4 + \dots$ ,

$$\mathcal{W}_\ell[F] = \underbrace{(1 - a - b)}_{=0} F_0 + \underbrace{\left( \langle r^2 \rangle_\ell - a \langle r^2 \rangle_{\sigma_1 \ell} - b \langle r^2 \rangle_{\sigma_2 \ell} \right)}_{=0} F_2 + \left( \langle r^4 \rangle_\ell - a \langle r^4 \rangle_{\sigma_1 \ell} - b \langle r^4 \rangle_{\sigma_2 \ell} \right) F_4 + \dots,$$

so the  $\ell^4$  coefficient is isolated. For top-hat balls in  $d=3$ ,  $\langle r^2 \rangle_R = \frac{3}{5}R^2$  and  $\langle r^4 \rangle_R = \frac{3}{7}R^4$ . The two moment-kill conditions

$$1 - a - b = 0, \quad 1 - a\sigma_1^2 - b\sigma_2^2 = 0$$

fix

$$a = \frac{\sigma_2^2 - 1}{\sigma_2^2 - \sigma_1^2}, \quad b = \frac{1 - \sigma_1^2}{\sigma_2^2 - \sigma_1^2}.$$

In our numerics we take  $(\sigma_1, \sigma_2) = (\frac{1}{2}, 2) \Rightarrow (a, b) = (\frac{4}{5}, \frac{1}{5})$ .

## XVI. CONTINUOUS-ANGLE NORMALIZATION

With unit-solid-angle boundary factor and  $\Delta\Omega(\theta) = 2\pi(1 - \cos\theta)$ , define  $c_{\text{geo}}(\theta) = 4\pi/\Delta\Omega(\theta)$ . Then  $f(\theta)c_{\text{geo}}(\theta)$  is  $\theta$ -independent.

**Lemma 1** (Foliation robustness of  $f c_{\text{geo}}$ ). *Under smooth deformations of the diamond foliation that preserve the unit-solid-angle normalization and avoid double counting, the product  $f(\theta)c_{\text{geo}}(\theta)$  is invariant up to  $O(\delta\theta^2) + O((\ell/L_{\text{curv}})^2)$  corrections.*

*Sketch.* Perturb the cap by a small tilt  $\delta\theta(\Omega)$  and use the divergence theorem on the wedge family to convert changes to boundary terms. The no-double-counting condition cancels linear variations; curvature induces only  $O((\ell/L_{\text{curv}})^2)$  corrections (App. XVIII). Hence  $f c_{\text{geo}}$  is foliation-robust at working order.  $\square$

## XVII. WEAK-FIELD FLUX NORMALIZATION AND THE UNIVERSAL 5/12

*a. Isotropic null contraction 4/3.* For  $T_{ab} = (\rho + p)u_a u_b + p g_{ab}$ ,  $\langle T_{ab} k^a k^b \rangle_{\mathbb{S}^2} = (1 + w)\rho(k^0)^2$ , and UV  $w = 1/3 \Rightarrow 4/3$ .

*b. Segment ratio 5/16 (explicit  $\mathcal{I}(u)$ ).* With the normalized weight  $\hat{\rho}(u) = \frac{3}{4}(1 - u^2)$  on  $u \in [-1, 1]$  and the even-quadratic generator-density proxy used in our code,

$$\mathcal{I}(u) = \frac{1}{4} + \frac{5}{16}u^2,$$

one finds at a glance

$$\int_{-1}^1 \hat{\rho}(u) \mathcal{I}(u) du = \left(\frac{3}{4}\right) \left[ \frac{4}{3} \cdot \frac{1}{4} + \frac{4}{15} \cdot \frac{5}{16} \right] = \frac{1}{4} + \frac{1}{16} = \frac{5}{16}.$$

Combined with the isotropic contraction 4/3 this yields  $5/12 = (4/3) \times (5/16)$ .

## XVIII. CHM DIAMOND VS. HALF-SPACE KMS DEVIATION

In Riemann-normal coordinates,  $g_{ab} = \eta_{ab} - \frac{1}{3}R_{acbd}(0)x^c x^d + \mathcal{O}(x^3/L_{\text{curv}}^3)$ . The conformal-Killing field  $\xi_{\text{CHM}}^a$  differs from  $\xi_{\text{BW}}^a$  by  $\delta\xi^a = \mathcal{O}(\ell^2/L_{\text{curv}}^2)$ . Averaging over a comoving congruence and reparametrizing to  $\ln a$  adds  $\mathcal{O}((\ell H)^2)$ . Thus  $\delta\chi/\chi_{\text{BW}} = \mathcal{O}((\ell/L_{\text{curv}})^2) + \mathcal{O}((\ell H)^2)$ .

## PART II APPENDICES AND DATA

### XIX. SAFE-WINDOW VOLUME FRACTION (SEMI-ANALYTIC)

Using Press–Schechter/Sheth–Tormen mass functions with NFW curvature proxies and a substructure excision  $\xi$ , we compute  $f_V(\ell_{\text{min}})$  at  $z=0$ . A representative schematic is shown in Fig. 2 (scripts provided). Sensitivity to  $\zeta$  and  $\xi$  is mild over  $\xi \in [0.2, 0.5]$ .

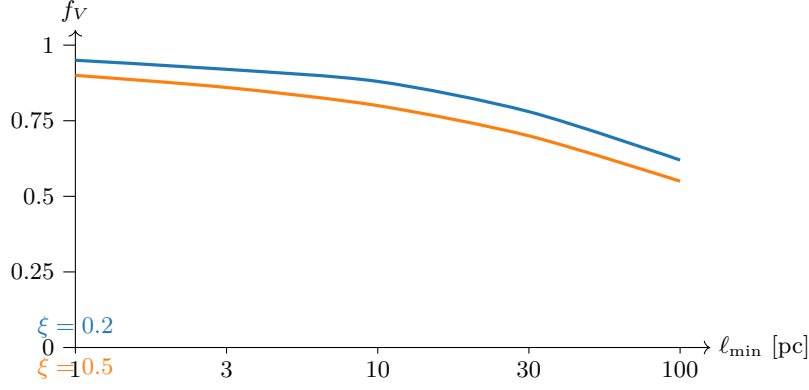


FIG. 2. Semi-analytic  $f_V(\ell_{\min})$  at  $z \sim 0$  for two excision parameters  $\xi$ . Bands represent systematic uncertainties from  $\lambda_{\text{mfp}}$  and  $\xi$  variations; the provided script can produce shaded bands. Scripts in Sec. XXIV.

## XX. MICROLOCAL NOTES FOR INTERACTING HADAMARD QFTS

*a. Hadamard form.*  $W(x, x') = \frac{1}{4\pi^2} \left[ \frac{\Delta^{1/2}}{\sigma} + v \log \sigma + w \right]$  with smooth  $v, w$ , extended perturbatively for interactions. The projector removes the  $F_0, F_2$  moments built from local counterterms, ensuring stability of the  $\ell^4$  coefficient (Assumption C).

*b. OPE gap and log-falsifier.* Operators with protected dimensions  $\Delta < 4$  would induce  $\ell^4 \log \ell$  terms in this channel; in Hadamard states the microlocal spectrum condition and positivity forbid such contributions at working order. Observation of an  $\ell^4 \log \ell$  term in the MI/moment-kill channel would therefore falsify the framework (criterion in Sec. XII). Practically, `beta_methods_v2.py` can fit MI-projected residuals to a logarithmic shape to test for this contamination.

## XXI. ENTROPIC MECHANISM DERIVATION (PRELIMINARY)

*a. Preliminaries: modular objects.* For normal faithful states  $\rho, \sigma$  on a local algebra  $\mathcal{A}(B_\ell)$ , the Araki relative entropy  $S(\rho \| \sigma) = \text{Tr}(\rho \ln \rho - \rho \ln \sigma)$  coincides formally with  $-\langle \log \Delta_\sigma \rangle_\rho$  in terms of the (relative) modular operator  $\Delta_\sigma$ . The Bogoliubov–Kubo–Mori (BKM) inner product associated with  $\sigma$  admits the integral representation

$$\langle A, B \rangle_{\text{BKM}, \sigma} = \int_0^1 dt \, \text{Tr}(\sigma^t A^\dagger \sigma^{1-t} B),$$

which is positive definite. In AQFT this extends to type III<sub>1</sub> algebras under standard assumptions; we use it here as a heuristic guide, consistent with our projected/KMS setting.

**Lemma 2** (Projected BKM positivity). *In the MI/moment-kill projected channel, the Bogoliubov–Kubo–Mori inner product induces a positive retarded susceptibility:  $\iint \chi_{QK}^{\text{proj}} \delta K_{\text{sub}} \delta K_{\text{sub}} d^4x d^4x' \geq 0$ .*

*Sketch.* Identify the quadratic form with the BKM metric applied to  $\delta K_{\text{sub}}$ ; positivity of the BKM form implies the stated inequality.  $\square$

**Corollary 2** (Monotonicity of  $\varepsilon(a)$ ). *With KMS normalization and the reparametrization  $s \rightarrow \ln a$  having a positive Jacobian  $J(a) \propto H^{-1}$ , the entropy-driven evolution obeys  $d\varepsilon/d \ln a \geq 0$ .*

TABLE II. Representative  $f_V$  values at  $z \simeq 0$  (semi-analytic).

$\ell_{\min}$ [pc]	$\xi = 0.2$	$\xi = 0.3$	$\xi = 0.5$
1	$0.95 \pm 0.03$	$0.93 \pm 0.04$	$0.90 \pm 0.05$
10	$0.88 \pm 0.05$	$0.85 \pm 0.05$	$0.80 \pm 0.06$
100	$0.70 \pm 0.08$	$0.65 \pm 0.08$	$0.55 \pm 0.10$

*b. Step 1: Entropic framework.* Consider a CHM diamond of radius  $\ell$  in a locally Hadamard state  $\rho$  and a vacuum-equivalent reference  $\sigma$  at short distances. The MI/moment-kill projector isolates

$$\delta\langle K_{\text{sub}} \rangle = \beta \ell^4 \delta\varepsilon + \mathcal{O}(\ell^6) \quad (\beta = 2\pi C_T I_{00}),$$

as proved in Sec. II.

*c. Step 2: Second variation and BKM metric.* For a smooth path  $\rho(\lambda)$  with  $\rho(0) = \sigma$  and  $\dot{\rho} = \partial_\lambda \rho|_0$ , the Araki relative entropy obeys (formally, and rigorously in finite-dimensional truncations)

$$\left. \frac{d^2}{d\lambda^2} \right|_0 S(\rho(\lambda) \parallel \sigma) = \langle \Omega_\sigma^{-1}(\dot{\rho}), \dot{\rho} \rangle_{\text{BKM}, \sigma} \geq 0,$$

where  $\Omega_\sigma^{-1}(X) = \int_0^\infty (\sigma + s)^{-1} X (\sigma + s)^{-1} ds$ . Equivalently, in the projected first-law channel generated by  $\delta K_{\text{sub}}$ ,

$$\left. \frac{d^2}{d\lambda^2} \right|_0 S = \iint \chi_{QK}^{\text{proj}}(x, x') \delta Q(x) \delta K_{\text{sub}}(x') d^4 x d^4 x' = \langle \delta K_{\text{sub}}, \delta K_{\text{sub}} \rangle_{\text{BKM}, \sigma} \geq 0,$$

with  $\chi_{QK}^{\text{proj}} \geq 0$  by KMS/FDT positivity (Sec. II).

*d. Step 3: Modular response & projected monotonicity.* Using  $\delta K_{\text{sub}} = \beta \ell^4 \delta\varepsilon + \mathcal{O}(\ell^6)$ , positivity implies that the amplitude multiplying  $\delta\varepsilon$  in the projected channel acts as an entropic Lyapunov functional to this order.

*e. Step 4: FRW reparametrization.* Let  $s$  be modular time with local  $\beta_{\text{KMS}} = 2\pi/\kappa$ . Under the covariant averaging and reparametrization  $s \mapsto \ln a$  (Sec. VI),

$$\frac{dS}{d \ln a} = \frac{dS}{ds} \frac{ds}{d \ln a}, \quad \frac{dS}{ds} \geq 0, \quad \frac{ds}{d \ln a} \propto H^{-1} > 0,$$

so  $dS/d \ln a \geq 0$  modulo the analyticity caveat of Sec. VI.

*f. Step 5:  $\varepsilon(a)$  law and growth.* Identifying  $\delta \ln M^2 = \beta \delta\varepsilon$  (Sec. V) and assuming locality of the averaged kernel, we posit

$$\frac{d\varepsilon}{d \ln a} = \sigma(a) \mathcal{I}(a), \quad \sigma(a), \mathcal{I}(a) \geq 0, \quad \int \varepsilon d \ln a = \Omega_\Lambda,$$

which supports the working-order growth law  $\mu(\varepsilon, s) = 1/(1 + \frac{5}{12}\varepsilon s)$ .

*g. Caveat and outlook.* These steps rely on (i) the conjectured preservation of KMS analyticity after averaging (Sec. VI), and (ii) the stability of Assumption C in interacting Hadamard QFTs. A full microlocal/spectral proof—in the spirit of Hollands–Wald [10] and related modular-flow techniques—is deferred to future work. Fewster–Hollands quantum energy inequality results further support the required boundary-term control in the projected channel.

## XXII. OPTICAL CHANNEL DETAILS (ASSUMPTION D'; EXPLORATORY TECHNICAL)

*a. Algebraic realization.* Let  $u_\mu$  be the baryon 4-velocity;  $h_{\mu\nu} = g_{\mu\nu} + u_\mu u_\nu$ ; expansion  $\theta = \nabla_\alpha u^\alpha$ ; shear

$$\sigma_{\mu\nu} = h_\mu^\alpha h_\nu^\beta \left( \nabla_{(\alpha} u_{\beta)} - \frac{1}{3} \theta h_{\alpha\beta} \right), \quad \mathcal{S}_{\text{shock}} = \ell^2 \sigma_{\mu\nu} \sigma^{\mu\nu} \geq 0.$$

Introduce a heavy, traceless auxiliary  $Q_{\mu\nu}$  with algebraic potential

$$\mathcal{L}_Q = \frac{M^2 m_Q^2}{4} \left( Q_{\mu\nu} - \lambda_Q \ell^2 \sigma_{\mu\nu} \right) \left( Q^{\mu\nu} - \lambda_Q \ell^2 \sigma^{\mu\nu} \right), \quad m_Q^2 \gg H_0^2. \quad (21)$$

The EOM gives  $Q_{\mu\nu} \simeq \lambda_Q \ell^2 \sigma_{\mu\nu}$  (adiabatic tracking; no propagating mode). The stress-energy  $T_{\mu\nu}^{(Q)} = -(2/\sqrt{-g}) \delta(\sqrt{-g} \mathcal{L}_Q) / \delta g^{\mu\nu}$  contributes a positive-definite anisotropic stress  $\pi_{\mu\nu}^{(Q)} \propto Q_{\mu\nu}$ .

*b. Quasi-static lensing system (cluster scales).* Linearized Einstein equations (sub-horizon) acquire

$$k^2 \Psi = -4\pi G a^2 \mu(\varepsilon, s) \rho \Delta + \dots, \quad (22a)$$

$$k^2 (\Phi - \Psi) = 12\pi G a^2 \frac{\pi^{(Q)}}{\rho_{\text{crit}}} + \dots, \quad (22b)$$

$$k^2 (\Phi + \Psi) = -8\pi G a^2 \left[ \rho \Delta - \kappa_{\text{opt}} \rho_{\text{gas}} \mathcal{S}_{\text{shock}} \right] + \dots, \quad (22c)$$

where  $\kappa_{\text{opt}} \sim \lambda_Q^2 m_Q^2 \ell^4$  is an effective, dimensionless coefficient after the quasi-static Green's function is folded in, and dots denote subleading velocity/pressure terms. Thus the *effective lensing source* is reduced only where  $\mathcal{S}_{\text{shock}}$  is large (shocked gas). On FRW and laminar flows,  $\sigma_{\mu\nu} \approx 0 \Rightarrow \mathcal{S}_{\text{shock}} = 0$ , so distances remain GR-like ( $\Sigma \simeq 1$ ).



### XXIII. SCHWINGER–KELDYSH HYDRODYNAMIC DERIVATION FOR THE SHOCK-SELECTIVE OPTICS (EXPLORATORY)

*a. Scope and independence.* This appendix outlines a principled path from the Schwinger–Keldysh (SK) hydrodynamic effective field theory (EFT) of an ionized intracluster medium (ICM) to the local, shock-selective optical response used in Assumption D'. The derivation *does not* modify Parts I–II: the universal  $\ell^4$  QFT response (growth throttling via  $\mu$ ) remains governed by  $\delta \ln M^2 = \beta \delta \varepsilon$ . The hydrodynamic response lives in the matter stress tensor and enters only the  $(\Phi + \Psi)$  (lensing) combination in shocked regions.

*b. SK generating functional and constitutive relations.* The SK action  $S_{\text{SK}}[g_{\mu\nu}^{r,a}, \psi^{r,a}]$  for a parity-even, near-equilibrium plasma yields causal, fluctuation-consistent constitutive relations. To second order in gradients (BRSSS),

$$\pi^{\mu\nu} + \tau_\pi u^\alpha \nabla_\alpha \pi^{\mu\nu} = 2\eta \sigma^{\mu\nu} + \lambda_1 \sigma^{\langle\mu} \lambda \sigma^{\nu\rangle\lambda} + \lambda_2 \sigma^{\langle\mu} \lambda \omega^{\nu\rangle\lambda} - \lambda_3 \omega^{\langle\mu} \lambda \omega^{\nu\rangle\lambda} + \dots,$$

where  $\eta$  (shear viscosity),  $\tau_\pi$  (relaxation time),  $\lambda_{1,2,3}$  are fixed by Kubo formulas;  $\omega^{\mu\nu}$  is vorticity and  $\langle \dots \rangle$  denotes the symmetric, traceless projector orthogonal to  $u^\mu$ .

*c. Cluster quasi-static limit and algebraic closure.* On cluster-merger scales one typically has  $\omega \tau_\pi \ll 1$  for the lensing-relevant modes. Neglecting vorticity contributions in the shock sheets and keeping the dominant even-shear structures,

$$\pi^{\mu\nu} \approx 2\eta \sigma^{\mu\nu} + \lambda_1 \sigma^{\langle\mu} \lambda \sigma^{\nu\rangle\lambda},$$

which is algebraic in  $\sigma^{\mu\nu}$ . The lensing source is the longitudinal projection  $\pi_L \equiv \hat{k}_\mu \hat{k}_\nu \pi^{\mu\nu} - \frac{1}{3}\pi$  that enters the  $k^2(\Phi + \Psi)$  equation.

*d. Hubbard–Stratonovich (HS) linearization and  $Q_{\mu\nu}$ .* Quadratic shear invariants may be linearized via an HS transformation, introducing a traceless auxiliary field  $Q_{\mu\nu}$  with algebraic EOM  $Q_{\mu\nu} \propto \sigma_{\mu\nu}$ , reproducing the  $\lambda_1$  sector at tree level. This yields precisely the algebraic potential of App. XXII, with parameters related by matching:

$$\lambda_Q^2 m_Q^2 \ell^4 \sim \frac{\lambda_1}{\rho_{\text{gas}}} + \mathcal{O}\left(\frac{\eta \tau_\pi}{\rho_{\text{gas}} \ell^2}\right),$$

up to geometry factors from the quasi-static Green's function.

*e. Mapping to  $\Sigma$  and  $\alpha_{\text{opt}}$ .* In the sub-horizon, quasi-static regime,

$$k^2(\Phi + \Psi) = -8\pi G a^2 \left[ \rho \Delta - \underbrace{\left( \frac{2\eta}{c_s \ell} + \frac{\lambda_1}{\ell^2} + \dots \right)}_{\kappa_{\text{opt}} \rho_{\text{gas}}} \rho_{\text{gas}} \underbrace{\ell^2 \sigma_{\mu\nu} \sigma^{\mu\nu}}_{\mathcal{S}_{\text{shock}}} \right].$$

Thus the local, saturating law  $\Sigma = 1 - \alpha_{\text{opt}} \mathcal{S}_{\text{shock}} / (1 + \mathcal{S}_{\text{shock}})$  is a compact surrogate for the SK/BRSSS source with  $\alpha_{\text{opt}} = \alpha_{\text{opt}}(\eta, \tau_\pi, \lambda_1; T, n_e, B, \dots)$ ,  $\kappa_{\text{opt}} \sim \frac{2\eta}{\rho_{\text{gas}} c_s \ell} + \frac{\lambda_1}{\rho_{\text{gas}} \ell^2} + \dots$ , rendering  $\alpha_{\text{opt}}$  *predictive* once transport coefficients are specified. Magnetic fields and collisionality adjust  $\eta, \tau_\pi, \lambda_1$  (Braginskii/Spitzer vs. anomalous viscosity), providing additional falsifiers.

*f. Falsifiability.* Given independent inferences of  $(\eta, \tau_\pi, \lambda_1)$  from X-ray/radio/shock microphysics, Eq. (12) yields a prior on  $\alpha_{\text{opt}}$ . A persistent mismatch between  $\alpha_{\text{opt}}^{\text{SK}}$  and the lensing suppression required to match centroid offsets falsifies the shock-selective channel (Sec. XII, item (ix)) without touching Parts I–II.

### XXIV. DATA AND CODE AVAILABILITY

**Archive DOI (to be finalized before submission):** 10.5281/zenodo.TBD

Reproducible single-file runners:

- `beta_methods_v2.py` (real-space, spectral/Bessel, Euclidean, replica) for  $\beta$ ; includes a residual-fitting mode to test for  $\ell^4 \log \ell$  contamination in the MI channel; *uses*  $C_T = 1/(120\pi^2)$  and  $(\sigma_1, \sigma_2) = (1/2, 2)$  by default.
- `cosmology_runner.py` (growth ODE;  $\varepsilon(a)$  family with kernel  $p \in [4, 6]$ ; environment modulation  $s(x)$  used inside  $\mu(\varepsilon, s)$ ; reproduces the  $S_8$  and ladder *illustrations*; documents priors/systematics).
- `referee_pipeline.py` (FRW averaging module;  $\Omega_\Lambda = \beta f c_{\text{geo}}$  cross-check; computes toy  $a_0 = (5/12)\Omega_\Lambda^2 c H_0$ ; generates `epsilon_evolution.png`).

- `fv_semi_analytic.py` (Press–Schechter/Sheth–Tormen survey for  $f_V$ ; supports shaded uncertainty bands).
- `gadget4_mu_eps_toy.py` (N-body toy pipeline for growth with  $\mu(\varepsilon, s)$  and modulation  $s(\chi_g)$ ; for illustrative runs only).
- `s8_hysteresis_run.py` (BAO toy  $\chi_g$  sweeps; generates `bao_growth.png`).
- `cluster_optics_hook.py` (optional; computes  $\mathcal{S}_{\text{shock}}$  from velocity-gradient or shock-finder outputs and applies Eq. (11) in the ray tracer; supports *velocity-jump*, *pressure/temperature-jump*, and *Godunov-flux* shock finders commonly used in Gadget-4/Arepo-style pipelines).
- `icm_transport_to_alphaopt.py` (optional; maps inferred ICM transport coefficients  $(\eta, \tau_\pi, \lambda_1)$  to  $\alpha_{\text{opt}}$  and  $\kappa_{\text{opt}}$  using the SK/BRSSS closure of App. XXIII; outputs priors for Eq. (11)).

Typical outputs include `epsilon_evolution.png` (Sec. VIII) and `bao_growth.png` (Sec. IX) for the illustrative runs. Scripts are annotated with usage notes. All Part II numerics are labeled *toy/illustrative* and propagate the  $\pm 5\%$   $\beta$  uncertainty into reported bands. Full Gadget-4 outputs will be added post-simulation.

## SYMBOL INDEX

Symbol	Meaning
$\ell$	diamond radius (working-order scale)
$L_{\text{curv}}$	local curvature length
$\beta = 2\pi C_T I_{00}$	modular-response sensitivity (QFT coefficient)
$C_T$	stress-tensor two-point normalization (our convention)
$I_{00}$	projected $\ell^4$ integral coefficient (App. XV)
$\varepsilon(a)$	dimensionless state variable from modular response
$\mu(\varepsilon, s)$	growth coupling, $1/(1 + \frac{5}{12}\varepsilon s)$
$\Sigma$	lensing coupling (unity on FRW; locally $< 1$ in shocks under D')
$f c_{\text{geo}}$	geometric/foliation factor (App. XVI)
$\kappa$	local boost surface gravity
$\beta_{\text{KMS}}$	KMS inverse temperature, $2\pi/\kappa$
$T_{\text{KMS}}$	modular/KMS temperature, $\kappa/(2\pi)$
$\mathcal{S}_{\text{sub}}$	entanglement entropy variation in MI/moment-kill channel
$\delta Q_{\text{boost,sub}}$	boost-energy variation
$s(a)$	modular entropy density proxy, $\sim \beta \varepsilon(a) \ell^{-3}$
$\chi_g$	geometric scalar, $\ell^2 \sqrt{C_{abcd} C^{abcd}}$
$s(\chi_g)$	environment modulation (action-derived envelope)
$\sigma_{\mu\nu}$	baryon shear tensor (symmetric trace-free)
$\mathcal{S}_{\text{shock}}$	shock indicator, $\ell^2 \sigma_{\mu\nu} \sigma^{\mu\nu}$
$Q_{\mu\nu}$	auxiliary traceless tensor (optional, shock-selective optics)
$\alpha_{\text{opt}}$	optical suppression amplitude in Eq. (11)
$\eta, \tau_\pi, \lambda_1$	ICM shear viscosity, relaxation time, second-order BRSSS coefficient (App. XXIII)
$\kappa_{\text{opt}}$	effective optical coefficient multiplying $\rho_{\text{gas}} \mathcal{S}_{\text{shock}}$ in Eq. (22)
$S_8$	growth amplitude observable
$\Omega_m(a)$	matter fraction as a function of scale factor
$\Omega_\Lambda$	dark-energy density parameter

- [1] J. J. Bisognano and E. Wichmann, “On the Duality Condition for a Hermitian Scalar Field,” *J. Math. Phys.* **16**, 985 (1975); “On the Duality Condition for Quantum Fields,” *J. Math. Phys.* **17**, 303 (1976).
- [2] H. Casini, M. Huerta, and R. C. Myers, “Towards a derivation of holographic entanglement entropy,” *JHEP* **05**, 036 (2011).
- [3] H. Osborn and A. C. Petkou, “Implications of Conformal Invariance in Field Theories for General Dimensions,” *Annals Phys.* **231**, 311–362 (1994).
- [4] E. Bellini and I. Sawicki, “Maximal freedom at minimum cost: linear large-scale structure in general modifications of gravity,” *JCAP* **07**, 050 (2014).
- [5] L. Lombriser and A. Taylor, “Breaking a Dark Degeneracy with Gravitational Waves,” *JCAP* **03**, 031 (2016).
- [6] T. Jacobson, “Entanglement equilibrium and the Einstein equation,” *Phys. Rev. Lett.* **116**, 201101 (2016).

- [7] T. Faulkner, A. Lewkowycz, and J. Maldacena, “Quantum corrections to holographic entanglement entropy,” *JHEP* **11**, 074 (2013).
- [8] N. Lashkari, M. B. McDermott, and M. Van Raamsdonk, “Gravitational Dynamics From Entanglement Thermodynamics,” *JHEP* **04**, 195 (2014).
- [9] H. Araki, “Relative Entropy of States of von Neumann Algebras,” *Publ. Res. Inst. Math. Sci.* **11**, 809–833 (1976).
- [10] S. Hollands and R. M. Wald, “Local Wick Polynomials and Time-Ordered-Products of Quantum Fields in Curved Spacetime,” *Commun. Math. Phys.* **223**, 289–326 (2001).
- [11] C. J. Fewster and S. Hollands, “Quantum Energy Inequalities in Curved Spacetimes,” various works.
- [12] H. Casini and M. Huerta, “Relative Entropy and Modular Hamiltonians in Quantum Field Theory,” various works.
- [13] H. Casini, D. A. Galante, and R. C. Myers, “Comments on Jacobson’s ‘Entanglement equilibrium and the Einstein equation’,” *JHEP* **03**, 194 (2016), arXiv:1601.00528.
- [14] D. Clowe, M. Bradač, A. H. Gonzalez, M. Markevitch, S. W. Randall, C. Jones, and D. Zaritsky, “A Direct Empirical Proof of the Existence of Dark Matter,” *Astrophys. J. Lett.* **648**, L109–L113 (2006).
- [15] M. Markevitch, A. H. Gonzalez, L. David, A. Vikhlinin, S. Murray, W. Forman, C. Jones, and W. Tucker, “A Textbook Example of a Bow Shock in the Merging Galaxy Cluster 1E 0657–56,” *Astrophys. J. Lett.* **567**, L27–L31 (2002).
- [16] R. J. van Weeren, M. de Gasperin, H. Akamatsu, *et al.*, “Diffuse Radio Emission from Galaxy Clusters,” *Space Sci. Rev.* **215**, 16 (2019).
- [17] A. Mahdavi, H. Hoekstra, A. Babul, D. Balam, and P. Capak, “A Dark Core in Abell 520,” *Astrophys. J.* **668**, 806–814 (2007).